Reprinted from *J. Mol. Biol.* (1994) **238**, 214–225

Solution Structure of GDP-tubulin Double Rings to 3 nm Resolution and Comparison with Microtubules

J. Fernando Díaz, Emmanuel Pantos, Joan Bordas and Jose M. Andreu

WITH AN APPENDIX

Hydrodynamic Analysis of Tubulin Dimer and Double Rings

Jose Garcia de la Torre and Jose M. Andreu

J. Mol. Biol. (1994) **238**, 214–225

Solution Structure of GDP-tubulin Double Rings to 3 nm Resolution and Comparison with Microtubules

J. Fernando Díaz[1], Emmanuel Pantos[2], Joan Bordas[2] and Jose M. Andreu[1]†

[1]*Centro de Investigaciones Biológicas, C.S.I.C. Velazquez 144, 28006 Madrid, Spain*

[2]*S.E.R.C. Daresbury Laboratory, Warrington WA4 4AD, U.K.*

GDP liganded tubulin, which is inactive in microtubule assembly, polymerizes into rings more readily than the active GTP liganded protein. The structure of double rings made of highly purified GDP-tubulin has been characterized to 3 nm resolution with synchrotron X-ray solution scattering. The scattering profile has characteristic maxima due to closely packed double rings of 38 nm mean diameter, with a 5·5 nm mean spacing between the rings, and a 4·2 nm centre-to-centre spacing between non-globular tubulin monomers within both rings. There are probably 24 and 32 monomers in the inner and outer ring, respectively, and the double ring population is more than 75% homogeneous in size. Comparison of this double ring structure to the lattice of tubulin molecules in microtubules indicates that the tubulin rings are equivalent to pairs of protofilament segments curved tangentially to the microtubule surface, with bending angles of 30° and 22·5° per tubulin $\alpha\beta$ dimer. When the rings are modelled employing the same non-globular tubulin monomer as in microtubules, the best computer fitted scattering profiles correspond to monomer orientations equivalent to two microtubule protofilaments coiled sideways, with same or opposite polarity. Rings constitute the equilibrium assembly state of GDP-tubulin, which is tensioned inside microtubules after GTP hydrolysis, causing their functional instability. In analogy with other nucleotide binding proteins, the inactive/active structural switch of tubulin is induced by the binding of the gamma phosphate and a coordinated Mg ion. It should involve domain rearrangements which cancel the bending of the tubulin dimer in the ring structure.

Keywords: tubulin rings; microtubules; GDP; GTP; X-ray solution scattering

1. Introduction

(a) *Why study GDP-tubulin rings?*

The $\alpha\beta$-tubulin dimer contains two GTP-Mg^{2+} binding sites. The GTP bound to the α subunit is non-exchangeable, while one exchangeable GTP bound to the β subunit (E site) is hydrolysed to GDP and P_i following the polar assembly of the tubulin dimer into microtubules. Microtubules and their associated proteins and motors are essential to cellular architecture, organelle transport and cell division. Tubulin in microtubules will not exchange the nucleotide until microtubule disassembly, or at the microtubule plus end (Erickson & O'Brien, 1992; Mitchison, 1993). While GTP-tubulin is the active form of the protein, GDP-tubulin is inactive and will not normally assemble into microtubules. Thus, the body of microtubules, which normally consists of inactive GDP liganded protein, is intrinsically unstable and is prevented from disassembly by interaction with the active GTP-tubulin terminal cap (Carlier, 1991). The stochastic loss and recovery of the stabilizing cap generate the length fluctuations characteristic of microtubule dynamic instability (Kirschner & Mitchison, 1986; Chen & Hill, 1985; Erickson & O'Brien, 1992; Martin *et al.*, 1993). Non-hydrolysable GTP analogues with γ-phosphate groups capable of proper coordination with Mg^{2+} support microtubule assembly (Shearwin & Timasheff, 1992; Hyman *et al.*, 1992), and nucleotide hydrolysis is believed to be required to destabilize microtubules (Carlier *et al.*, 1988). Microtubule instability, also observed *in vivo* (Cassimeris *et al.*, 1988), is currently thought to be employed by the cell to regulate in space and time the assembly of these structures (Kirschner & Mitchison, 1986; Verde *et al.*, 1992). Clearly, the interactions of the exchangeable nucleotide γ-phosphate and a coordinated magnesium ion with the protein control the molecular switch of tubulin functionality and microtubule dynamic instability.

Tubulin undergoes a magnesium-induced isodesmic self-association leading to formation of characteristic 42 ± 2 S double rings (Frigon &

† Author to whom all correspondence should be addressed.

0022-2836/94/170214-12 $08.00/0

Timasheff, 1975*a*,*b*). Slight modification of the ring-forming solution conditions led to the discovery of the self-assembly of purified tubulin into microtubules (Lee & Timasheff, 1975). It has been shown that the apparent affinity of the ring closure reaction of GDP-tubulin is more favourable than that of GTP-tubulin by −50 to −75 kJ/mol, that is, GDP-tubulin appears to coil better (Howard & Timasheff, 1986; Shearwin & Timasheff, 1992). This and the observation that cold depolymerization of microtubules to double rings proceeds *via* formation of curved oligomers, have led to the proposal that while GTP-tubulin is in a "straight" active microtubule forming conformation, GDP-tubulin is in an inactive "curved" ring-favouring conformation (Melki *et al.*, 1990; Timasheff, 1991). Therefore, tubulin rings can be regarded as the relaxed assembly state of tubulin, corresponding to tubulin in the body of microtubules if their stabilization was relieved. Since the GDP-tubulin and the GTP-tubulin dimers are essentially indistinguishable by most solution techniques (J.F.D., E.P., J.B. & J.M.A., unpublished results), and the high resolution three-dimensional structure of tubulin is currently unavailable, the only way to study their structural differences is by their propagated properties, that is, by comparison of the structures of rings and microtubules. The low resolution structure of microtubules is known from electron microscopy image reconstruction (Amos & Klug, 1974), X-ray fibre diffraction (Mandelkow *et al.*, 1977; Beese *et al.*, 1987), and X-ray solution scattering methods (Bordas *et al.*, 1983; Andreu *et al.*, 1992). Tubulin rings, observed since the early days of microtubule assembly studies, have attracted considerable interest, though their substructure could hardly be discerned. The centre-to-centre distance between tubulin subunits in double rings, scarcely appreciable by electron microscopy (Frigon & Timasheff, 1975*a*; Scheele & Borisy, 1978; Voter & Erickson, 1979) and by X-ray scattering (Mandelkow *et al.*, 1983), is approximately 4 nm, consistent with the proposal that rings correspond to coiled protofilaments of microtubules (Kirschner *et al.*, 1974). The exact ring dimensions and spacings between the tubulin molecules, and their orientation within each ring relative to that in microtubules were unknown. This is important in order to eventually understand the molecular switch associated to GTP hydrolysis. In this study we have unequivocally determined the arrangement of protein subunits in purified GDP-tubulin double rings employing accurate synchrotron X-ray solution scattering methods and computer modelling, as well as a possible monomer shape, and compare the assembly topology of rings and microtubules.

2. Materials and Methods

(a) *Protein, X-ray scattering measurements and data reduction*

Highly purified tubulin was prepared from calf brain and its E-site nucleotide exchanged to give over 99% GDP-tubulin, in 10 mM sodium phosphate buffer, 1 mM ethylenediaminetetraacetic acid, 7 mM $MgCl_2$, 1 mM GDP, pH 6·7 (Díaz & Andreu, 1993). Time-resolved X-ray measurements of tubulin assemblies were performed to 2 nm spatial resolution at station 2.1 of the Daresbury Laboratory Synchrotron Radiation Source as described (Andreu *et al.*, 1989, 1992), employing a thermostatted scanning sample cell body made of beryllid instead of metal. The spacing between the mica windows was 1 mm and the volume of the sample was 0·7 ml. The distances between sample and detector were 6 m, 3 m and 1·5 m. Data were processed with a modified version of the program OTOKO (Koch & Bendall, 1981; Mant & J.B., unpublished results) in Unix workstations.

(b) *Theory*

The zero angle X-ray scattering of a solution of identical particles is proportional to their number concentration and the square of their scattering mass (volume times excess electron density: Guinier & Fournet, 1955). For a solution of polymerizing subunits, the forward scattering is proportional to the weight average degree of polymerization and, in practice, the scattering at very low angle (central scatter) constitutes a measure of the degree of polymerization in the sample, which will be sensitive to a given size interval depending on the geometry of the X-ray camera and detector (Bordas *et al.*, 1983). The X-ray scattering profiles of microtubules can be analysed by reference to their fibre diffraction diagrams, interpreted by helical diffraction theory as described elsewhere (Andreu *et al.*, 1992). The X-ray scattering pattern of rings can be qualitatively understood by considering them as one turn of a helix of nil pitch. For rings of diameter significantly larger than the distance between neighbouring monomers constituting them, and at the level of resolution we are concerned with, it is convenient to consider their X-ray scattering as consisting of 2 regions. At relatively low values of the scattering vector **S** (defined as a reciprocal Bragg spacing, i.e. $\mathbf{S} = 2(\sin\theta)/\lambda$, where 2θ is the scattering angle and λ is the X-ray wavelength employed, the pattern will be dominated by the X-ray scattering due to the excess electron density of the ring as a whole relative to its surroundings, while the diffraction effects due to the monomer arrangement within the ring will only show at higher angles. Thus, at low resolution the ring can be regarded as a section of a hollow cylinder, and its scattering pattern will show a series of bands corresponding to a J_0-like Bessel function with argument $\pi D\mathbf{S}$, where D is the diameter of the ring, though the position of these subsidiary maxima will not equal those of a true J_0, unless the height of the ring is greater than its radius. Two concentric rings will have an X-ray scattering pattern in which the position of these bands also follows the behaviour of a J_0-like Bessel function dictated by the mean diameter of the double ring. However, it is possible to distinguish between single and double concentric rings because, in the former, the intensity of the subsidiary maxima will decay monotonically with increasing angles, while in the latter, the intensities are modulated by the interference between the inner and the outer ring leading to the almost complete disappearance of some of the low-angle subsidiary maxima (roughly at a spacing equal to the thickness of the double ring) and to an enhancement in their prominence at higher angles. Stacks of rings, whether single or double, will not alter much the positions of these subsidiary maxima; however, the higher the stack the more prominent the subsidiary bands will be. At higher angles the

n-fold symmetry of the rings (where n is the number of subunits per ring) gives rise to a band corresponding to a J_n Bessel function, which is sensitive to the subunit spacing and shape, and which will have its first maximum roughly where the argument equals the order, i.e. at $\mathbf{S} \approx (n+1)/\pi D$. For rings made of slightly different numbers of equally spaced subunits, these **S** values will be close, because the different indexing is compensated by the change in diameter. Formation of ring stacks will also contribute to the scattering intensity in this region, due to the contacting subunits in different rings. On the other hand, tubulin rings may aggregate into 2-dimensional arrays. If this aggregation formed a bidimensional crystal, the X-ray solution diffraction pattern would be the rotationally averaged product of the scattering pattern of the ring by the transform of the lattice. The latter consists of diffraction rods in which the only values different from zero occur at the reciprocal vector positions of the 2-dimensional array. In solution, these diffraction rods would show up as diffraction bands gradually decaying at increasing angles. For a hexagonal array of objects, the centre-to-centre distance can be simply determined from the 1,0 lattice spacing (i.e. the reciprocal of the **S** value of the first diffraction maximum) divided by cos 30°. The absence of crystallographic sampling at high, but not low, angles (see Figure 2, band at 0·0258 nm^{-1}, which is not followed by more diffraction bands) is indicative of substantial disorder of the so-called second kind, in which the short-range order is retained (Vainshtein, 1966). This is characteristic of paracrystalline assemblies and includes rotations and shifts of the repeating motifs from the crystallographic positions, bending and distortion of the packing array. An approximate value of these distortion parameters can be deduced by inspecting at what resolution the transform of the repeating motif is no longer sampled by the lattice net points (Vainshtein, 1966).

(c) *Model calculations*

The X-ray scattering profiles of protein assemblies can be readily analysed by direct comparison with computer model calculations based on Debye's formula (Guinier & Fournet, 1955; Vainshtein, 1966; Bordas *et al.*, 1983; Mandelkow *et al.*, 1983; Wakabayashi *et al.*, 1992; Garrigos *et al.*, 1992). The tubulin assemblies were simulated employing the program LEGO (Pantos *et al.*, 1988). The tubulin monomer was represented by either a single sphere of 3 nm diameter (Mandelkow *et al.*, 1983), or the group of closely packed spheres of 1·2 nm radius previously employed to model the monomer within microtubules (Andreu *et al.*, 1992). The X-ray scattering profile of each assembly was calculated employing a solution scattering simulation program (DALAI, Pantos & Bordas, 1994) implemented on Unix computers. This program employs an optimized implementation of the Debye formula for models built of identical spheres. The speed of computation of the scattering profiles permits systematic scans of model parameters. The program can be executed in parallel on networked workstations (E.P., unpublished), permitting the simulation of X-ray scattering for larger systems. Accurate values of the rings' diameter were obtained by calculating the positions of the subsidiary maxima of the J_0-like Bessel function in ring models made up of a large number of spherical subunits. The positions of the first 10 maxima appeared at 0, 1·29, 2·31, 3·32, 4·33, 5·33, 6·33, 7·34, 8·34 and 9·34 times D^{-1}. These values are different from the corresponding coefficients derived from the J_0 Bessel function argument (0, 1·22, 2·23, 3·24, 4·24, 5·24, 6·24, 7·24, 8·25 and 9·25; Abramowitz & Stegun, 1965). They became equal to the Bessel coefficients for stacks of rings of height roughly larger than their radius. For rings made of 3 nm spherical subunits spaced between 4 and 8 nm, the computed positions of the maxima corresponding to the J_n Bessel function were comprised within the interval $\mathbf{S} = n/(2{\cdot}77 \pm 0{\cdot}11)D$. This allows direct measurement of the centre-to-centre distance between the subunits, $d = \pi D/n = (1{\cdot}13 \pm 0{\cdot}05)/\mathbf{S}$, for $12 < n < 36$.

X-ray scattering models necessary for the analysis of the tubulin ring data are shown in Figure 1. Curve 1 in panel (a) (continuous line) is the computed scattering profile of a single ring of 38 nm diameter, containing 28 solid spheres which represent 14 tubulin dimers. The calculated profile of a double ring of the same mean diameter is shown by curve 2. Curves 3 show the effects of modifying the spacing between the inner and outer ring while keeping the mean diameter constant. Curves 4 correspond to mixtures of double rings made of different numbers of monomers, maintaining the average diameter of the population constant. Curve 5, in panel (b), is the scattering profile of a double ring made of 28 spheres in each ring (different inter-monomer distances) and the same mean diameter as model 2. Curve 6 is the scattering profile of a triple ring, curve 7 that of an array of 4 double rings, and curve 8 of a stack of 4 rings.

3. Results

(a) *Low resolution structure of GDP-tubulin double rings in solution: dimensions and subunit spacing*

Figure 2 shows the solution X-ray scattering profile of suspensions of ring sheets assembled from purified GDP-tubulin with 7 mM $MgCl_2$ at 2 °C, and the inset is an electron micrograph of the specimen, which is similar to those described previously (Díaz & Andreu, 1993). The scattering profile is characterized by a steep central scattering, and a very low angle, sharp, diffraction peak of 0·0258 nm^{-1} superimposed onto a scattering band, the position of which is uncertain (~0·03 nm^{-1}). Another band at 0·058 nm^{-1} follows, and a third subsidiary band is visible at 0·086 nm^{-1}. At higher angles there are four prominent bands centred at 0·116, 0·143, 0·116 and 0·192 nm^{-1}, a broad band at 0·23 nm^{-1}, and an asymmetric band at 0·282 nm^{-1}. These features were induced by Mg^{2+}, were optimally observed at 7 to 11 mM $MgCl_2$, and strongly decreased upon back-exchange of GTP into the E site of tubulin (not shown).

The low resolution structure of the tubulin rings can be characterized from the positions and the relative intensities of these peaks, as follows. The diffraction peak arises from the interference effects of a pseudolattice of rings, and from its position an average centre-to-centre distance between the rings can be roughly estimated as 45 nm (Materials and Methods and Figure 1, curve 7). This peak was less noticeable in incompletely exchanged GDP-tubulin preparations, in which it increased with time in GDP containing buffer, in agreement with the observed partial polymerization of these preparations into ring sheets (Díaz & Andreu, 1993). The band at a position around 0·03 nm^{-1} and the following seven peaks correspond to the second,

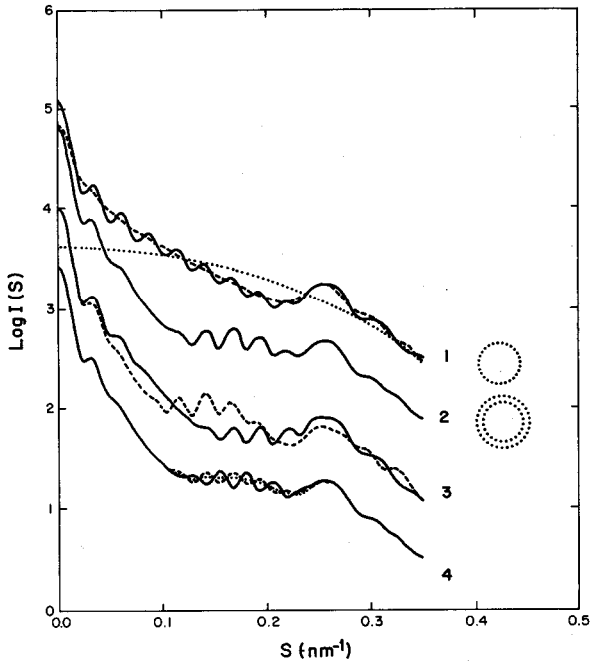

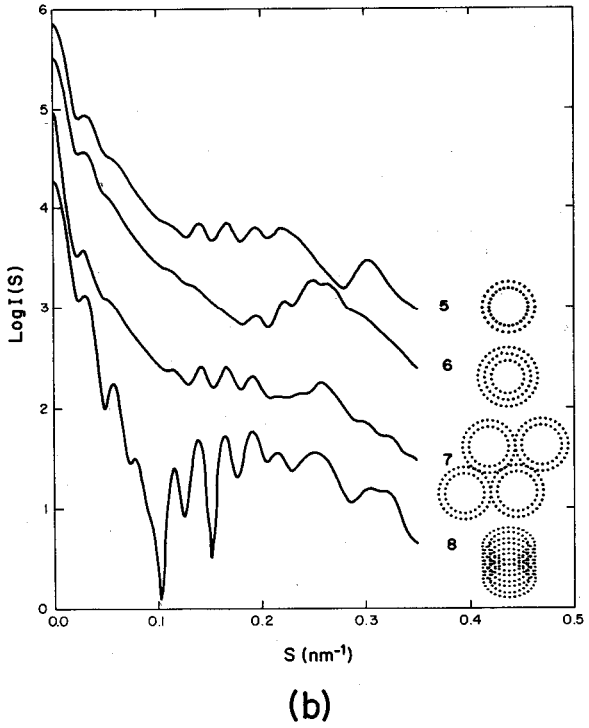

Figure 1. Computed X-ray solution scattering profiles of tubulin ring models of 38 nm mean diameter, made of solid spherical monomers of 3 nm diameter. (a) Curve 1: continuous line, single ring made of 28 monomers spaced 4·26 nm (i.e. 14 tubulin dimers); broken line, 14 monomers filling only one half of the ring (note the loss of the J_0 subsidiary maxima); dotted line, scattering profile of the spherical monomer. Curve 2: double ring of 32 and 24 monomers in the outer and inner ring, respectively, with the same spacing and mean diameter as above. The spacing between the inner and outer ring is 5·5 nm, note the modulation of the J_0 maxima by comparison to curve 1. Curve 3: continuous line, double ring as above, but the 24 monomer inner and the 32 monomer outer ring are spaced by 4·5 nm by slight modification (±0·13 nm) of the intermonomer spacings; broken line, inner and outer rings spaced 6·5 nm, note the marked displacement of the region of reinforcement of the J_0 subsidiary maxima by the changes in the inner-outer ring spacing. Curve 4: continuous line, a mixture of 75% double rings of 32 and 24 monomers (identical to curve 2) with 12·5% double rings of 30 and 22 monomers and 12·5% double rings of 34 and 26 monomers, note the displacement and change in intensity of the J_0 maxima with respect to curve 2; broken and dotted lines, same as the continuous line model mixture, but proportions modified to 0%:50%:50% and 50%:25%:25%, respectively. (b) Curve 5: double ring made of an equal number of 28 monomers unevenly spaced in the outer ring and inner ring, while keeping the mean diameter of the double ring constant; note the displacement of the J_0 maxima with respect to curve 2. Curve 6: triple ring made of 34, 28 and 22 monomers in the outer, middle and inner ring, respectively. Curve 7: array of 4 double rings identical to model 2 in a hexagonal lattice, obtained by superposition of outer ring monomers. Curve 8: stack of 4 double rings, spaced 8 nm along the cylinder axis.

third, fourth, etc. maxima of a J_0-like Bessel function, and arise from rings with a mean diameter of 38±1 nm (Materials and Methods). The intensity of such maxima in the calculated scattering profile of a single ring decays monotonically (Figure 1, curve 1), which does not correspond to the experiment, in which the intensity decays very fast in the second to fourth maxima, increasing again in the fifth, sixth, seventh and eighth maxima. This indicates that the structure is that of a double ring, in which the intensities of the different subsidiary maxima are modulated by the interference between the inner and the outer ring (Figure 1, curve 2). Comparison with models in which the distance between the inner and outer ring was modified (Figure 1, curves 3) indicated that in order to fit the interference (that is, the relative intensities of the different bands of the J_0-like Bessel function in that region), the spacing between the mean perimeters of both rings must be 5·5±0·5 nm. Therefore, the mean diameters of the inner and outer rings are 32·5±1 nm and 43·5±1 nm, respectively. The peak at 0·282 nm^{-1} corresponds to the J_n Bessel function for each ring of monomers, and its position indicates a centre-to-centre spacing of 4·0±0·2 nm for globular monomers (Materials and Methods). Models with larger intersubunit spacings, such as 5·5, 6, 7, 8 and 11 nm (not shown), were not compatible with the position of the J_n maxima. The number of spherical monomers in the outer-inner ring compatible with the data are 32 and 24, 34 and 26 or 36 and 28 (28, 30 or 32 tubulin dimers). Mixtures of one of these double ring types with more than 25% of next larger and next smaller possible sizes in equal proportions (Figure 1, curve 4) clearly fail to reproduce either the relative intensities of the J_0-like maxima or their positions, which indicates more than 75%

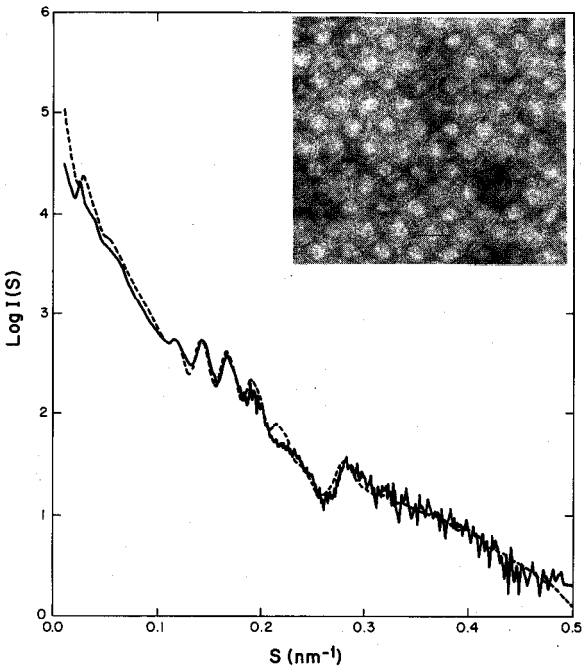

Figure 2. Continuous line, experimental X-ray solution scattering profile of GDP-tubulin in 7 mM $MgCl_2$ containing buffer (pH 6·7; see Materials and Methods) at 2 °C. The data are the averages of 2, 4 and 2 data sets, respectively, measured with 6 m, 3 m and 1·5 m camera lengths, employing 9 ± 2 mg/ml tubulin samples, and merged at superimposable zones near 0·075 nm^{-1} and 0·25 nm^{-1}. Broken line, computer fitted scattering profile of a hexagonal array of 4 double rings, each identical to the best ring model, which is shown in Figure 3(a). The ring centre-to-centre spacing is 43·5 nm. The scattering profile of the ring is modified due to diffraction-interference effects between rings, which is noticeable at low angle. There is also interference between monomers in the contact zones, which affects the profile at high angle, particularly in the 0·22 nm^{-1} and 0·28 nm^{-1} regions. Inset: representative negative stain electron micrograph of the sample; the bar corresponds to 50 nm.

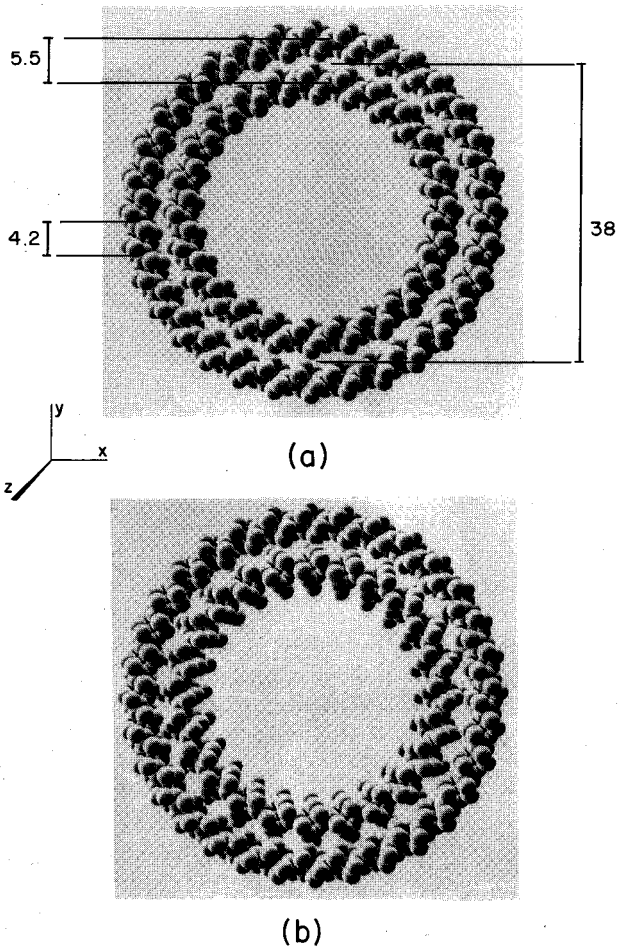

Figure 3. Computer models of tubulin double rings. The measured mean diameter, the centre-to-centre spacing between monomers within each ring, and the spacing between both rings are indicated in nm units. The outer and inner ring contain 32 and 24 monomers, respectively. Each tubulin monomer has been represented by a set of 21 solid spheres of 1·2 nm radius, previously employed to model the monomer in microtubules, and has been oriented to fit the data (see Materials and Methods) in (a) parallel or (b) antiparallel fashion.

homogeneity in size of the GDP-tubulin rings. Double rings with the same number of subunits (28, 30 or 32) unevenly spaced in the outer and inner ring could be built (Figure 1, curve 5), but they give J_n maxima incompatible with the data. In conclusion, the simple model described (Figure 1, curve 2) accounts for the general features of the scattering profile of the GDP-double rings, though it does not reproduce well the shape of the peaks and the steepness of the curve.

(b) *Tubulin monomer shape and orientation in double rings*

In order to better fit the double ring X-ray scattering data it becomes necessary to depart from spherical monomers. The tubulin monomers are known to be non-globular in microtubules (Amos & Klug, 1974; Beese *et al.*, 1987; Andreu *et al.*, 1992) as well as in dimers (Andreu *et al.*, 1989, and unpublished results). The spherical monomers were substituted by the tubulin monomer previously employed to model the scattering profile of microtubules (Andreu *et al.*, 1992), which is made of a set of small spheres within a roughly triaxial ellipsoidal envelope of axes approximately 4 nm × 7 nm × 8 nm. The monomer orientation was systematically varied in 10° steps, searching for the angles which fit the data. The best model found is shown by Figure 3(a). In this model the major axis of the monomer is perpendicular to the plane of the ring, and the middle axis deviates −60° from a radial position. The dimensions of the monomer in the X, Y, Z axes of the Figure are approximately 5·5 nm × 4 nm × 8 nm. Given the double ring dimensions and spacings, rotation of this monomer on the X and Z axes is hindered by the packing of subunits within each ring, and rotation on the Y

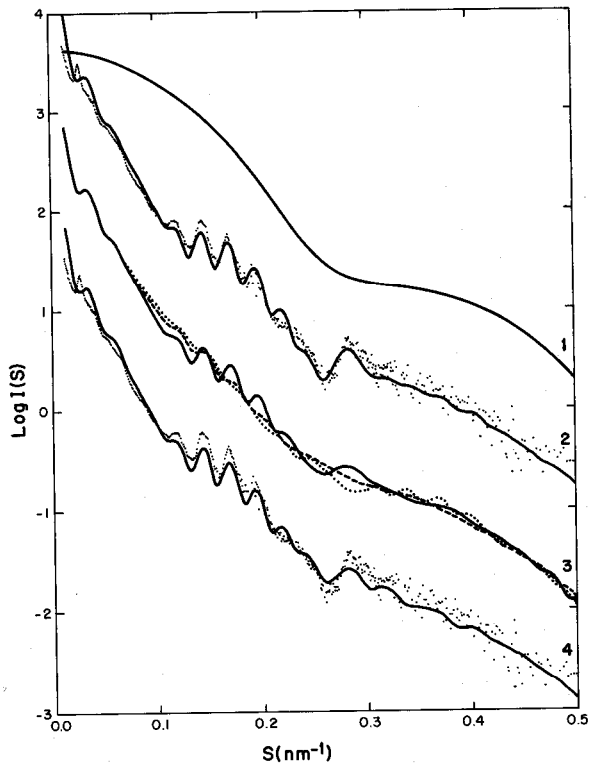

Figure 4. Fitting the X-ray solution scattering profile of GDP-tubulin by double rings made of non-spherical monomers. Curve 1, scattering profile of the tubulin monomer model employed; curve 2, computed scattering profile (continuous line) of best double ring model (Figure 3(a)) in comparison to the data (points). Note that in this modelling procedure, individual rings are not intended to reproduce the scattering features due to the formation of a ring pseudolattice in the sample, particularly the peak at 0·0258 nm^{-1}; curves 3, effects of rotating the tubulin monomer on the Y axis of Figure 3 by 30° (continuous line), 60° (broken line) and 90° (dotted line) with respect to the best fitting position (curve 2); curve 4, computed scattering profile (continuous line) of the antiparallel double ring model (Figure 3(b)) in comparison to the data (points).

axis is restricted by contact between subunits of both rings. Representative comparisons of model scattering profiles and the data are shown by Figure 4, continuous and dotted lines, respectively. Unrestricted rotation of the monomers on the Y axis can lead to fusion of the outer and inner rings, with a decrease in the intensities of the fifth, sixth, seventh and eighth J_0 maxima, among other effects. The best fits were obtained for angles of approximately 0° and 180° of the major axis of the monomer to the YZ plane, which are similar models at the model resolution (Figure 4, curve 2). Models deviating from these positions more than 20° were incompatible with the data (Figure 4, curves 3). Rotating the monomers on the X axis lead to monomer interpenetration in each ring, and loss of intensity and change in position of the J_n peak, because the rings became more uniform and the contrast due to the n-fold symmetry decreased. These models fitted reasonably the data at angles of 0° and 180°(±20°) of the major monomer axis to the XZ plane (not shown), which are identical structures (i.e. the double ring viewed from one or the other side). Rotation on the Z axis allowed fitting of the data at angles of the middle (7 nm) axis of the monomer to the XZ plane of 60° and 240° (which are identical models due to monomer symmetry) and less well at 120° and 300°. Positions deviating more than 15° from these values did not fit the data (not shown). It is also possible to position the monomers independently in each ring at the optimal angles described, generating several structures which are compatible with the data. Of these, the only structures clearly different from the best model (Figure 3(a) and Figure 4, curve 2) are those in which the outer and inner rings have opposite polarity, such as the antiparallel double ring model exemplified by Figure 3(b) and Figure 4 (curve 4). The diameter of the double ring, the number of monomers and the intermonomer spacings were refined to optimally fit the J_0 and J_n maxima. The mean diameter is 37·8 nm, the number of subunits in the outer and inner rings is 32 and 24, respectively, their spacing 4·24 nm, and the spacing between the inner and outer ring is 5·5 nm. All these values are within the experimental error of the first measurements.

Finally, if a small array of these double rings is constructed, a model scattering pattern can be generated (Figure 2, broken line) in which characteristics similar to the experimental double ring sheet appear (Figure 2, continuous line), though the interference maximum (0·0258 nm^{-1}) and the 0·22 nm^{-1} zone are not exactly reproduced due to the inherent difficulty in simulating a disordered large ring array. An explanation for the absence of more diffraction peaks is probably that only short range order is retained, and can be taken as an indication that the various possible distortions of the second kind lead to departures from the correct crystallographic positions for neighbouring rings at least of the size of the tubulin monomer (Materials and Methods). The values of the centre-to-centre distance between rings (best model fit 43·5 nm) and of the outer ring diameter (43·5 nm) imply superposition of outer rings in the pseudolattice. This is observed by electron microscopy (Figure 2, inset).

4. Discussion

(a) *Tubulin double ring structure*

Tubulin rings frequently form arrays which are only apparently ordered, and some of the ring preparations are heterogeneous, making image reconstruction studies difficult (J.M.A., J.B. & J. L. Carrascosa, unpublished results). However, objects with cylindrical symmetry can be very favourable for X-ray scattering study. Ring forming solutions of tubulin and associated proteins gave an X-ray scattering peak at 0·27 nm^{-1} (recorded on film after long exposure times), which was consistent with

ring models corresponding to coiled protofilaments (Mandelkow *et al.*, 1983). Employing a biochemically well-defined GDP-tubulin preparation which extensively forms Mg^{2+}-induced ring aggregates (Díaz & Andreu, 1993), sensitive synchrotron X-ray scattering instrumentation (Towns-Andrews *et al.*, 1989), and new X-ray scattering computer simulation procedures (Pantos & Bordas, 1994), it has now been possible to obtain measurements which we believe define unambiguously the solution structure of tubulin double rings to approximately 3 nm resolution, since hardly any other structure can be conceived which would give the same characteristic scattering profile (note that the measurements reach 2 nm resolution, though the absence of any detectable features between 3 and 2 nm resolution precludes any reliable assignment in this region). The determination of the ring dimensions and subunit spacings required no special assumptions about the shape of the monomers and was derived employing spherical monomers. Using spherical monomers, the number of subunits in the inner and outer ring could be 32 and 24, 34 and 26 or 36 and 28 from the X-ray scattering results. Since the number of tubulin molecules which associate to form the double rings, determined by sedimentation velocity with the same tubulin preparation under very similar conditions, is 26 ± 2 dimers (Frigon & Timasheff, 1975*a*; Howard & Timasheff, 1986), the GDP-tubulin rings are more probably made of 32 and 24 monomers in the outer and inner ring, respectively. Given the expected flexibility of linear tubulin oligomers, the detected homogeneity of the end product population of GDP-tubulin rings is remarkable.

The double ring scattering profile was modelled best employing tubulin monomers with a shape which fits the X-ray solution scattering of microtubules (Andreu *et al.*, 1992). The best fit was obtained with 32 and 24 monomers in the outer and inner ring, respectively. The simplest interpretation is that the monomer structure is not necessarily different in rings and microtubules at the resolution of these studies, though the intermonomer bonding interactions are not identical in both assemblies. The centre-to-centre spacing between monomers in rings appears to be approximately 0·2 nm larger than in protofilaments, which may result from the curvature of the structure. On the other hand, the formation of a ring pseudolattice perturbs the ring scattering profile, which makes difficult a more accurate modelling of the monomer shape.

(b) *Assembly topology of tubulin rings and microtubules and the molecular switch between inactive and active tubulin*

The low resolution structure of GDP-tubulin double rings and microtubules define unambiguously the relationship between both forms of protein self-assembly, assuming that the monomer dimensions are not drastically different in the two polymers. Since the spacing between monomers

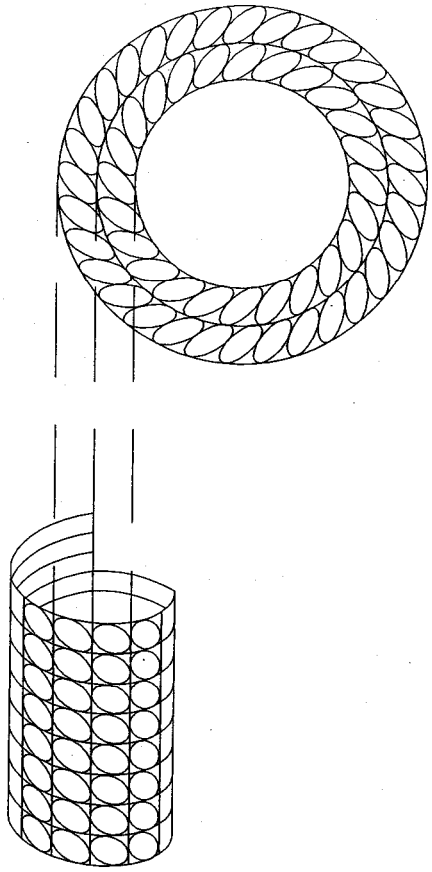

Figure 5. Assembly topology of GDP-tubulin rings and microtubules. The Figure represents 1 double ring (upper scheme) and 1 3-start microtubule lattice (lower scheme), in which the tubulin monomers are simply indicated by ellipsoids. Given the 4 nm longitudinal spacing and 5·5 nm lateral spacing between tubulin monomers in microtubules and double rings, the double ring geometrically corresponds to 2 fragments of neighbour protofilaments in the microtubule, coiled tangent to the microtubule surface, and circularly closed to contain 24 and 32 monomers, respectively, in the inner and outer ring. It should be noted that tubulin in the body of microtubules is in the GDP liganded form as in these rings.

along the rings is clearly 4 nm, the proposal that rings correspond to coiled protofilaments (Kirschner *et al.*, 1974; Voter & Erickson, 1979; Mandelkow *et al.*, 1983) is confirmed. The 5·5 nm spacing between the inner and outer ring is the same as the lateral spacing between protofilaments in microtubules (Andreu *et al.*, 1992). Therefore, the double rings correspond to two neighbour protofilaments curved. This is exemplified by Figure 5. The direction of coiling is most likely tangent to the microtubule surface (i.e. sideways), since coiling of one protofilament perpendicular to the microtubule surface (i.e. inside out) generates a ring of the same thickness as the microtubule wall (7 to 8 nm, Andreu *et al.*, 1992). Such a ring can either associate along its perimeter with another larger or smaller ring, giving a separation of 7 to 8 nm between both, or associate with an identical ring to form a stack of two, both of

which possibilities are incompatible with the data. Also, the best ring model was obtained with a monomer orientation which corresponds to protofilaments coiled tangent to the microtubule wall. This is not to mean that double rings form directly by lateral coiling of two protofilaments, since the ring formation from microtubules involves association of curved tubulin oligomers (Melki *et al.*, 1990). It has been reported that the ends of microtubules in the shrinking phase have coiled protofilaments with curvature similar to rings, while ends of growing microtubules have not, which could, in principle, be used to perform work in chromosome movement (Mandelkow *et al.*, 1991). In other cases, blunt depolymerizing ends were observed (Simon & Salmon, 1990) or their morphology was not specified (Wade *et al.*, 1989). The cryoelectron microscopy images of single coiling protofilaments at microtubule ends (Mandelkow *et al.*, 1991) suggest flexibility in the direction of coiling of single rings, which may become double rings by further protein association. Since having the same number of subunits in the inner and outer ring with different spacings between monomers in each of them is clearly incompatible with the data, the lateral contacts between monomers in the microtubule become necessarily out of register in the outer and inner rings with different numbers of subunits. Having 32 and 24 monomers in the outer and inner ring permits eight correct lateral interactions (Voter & Erickson, 1979). Lateral interactions are apparently conserved in microtubules with different protofilament numbers (Wade *et al.*, 1990; Andreu *et al.*, 1992; Ray *et al.*, 1993), which suggests that sliding lateral interactions in double rings should either be somehow different from microtubules, or play a minor role in the stability of the ring's structure.

The inactive GDP-tubulin forming the double rings can be readily made active in microtubule assembly by back-exchange of GTP (Díaz & Andreu, 1993). Since the affinity of Mg^{2+} for GDP-tubulin is much lower than for GTP-tubulin (Correia *et al.*, 1988), it is likely that the activation by GTP is linked to the binding to the E-site of β-tubulin of the nucleotide with its γ-phosphate and a coordinated divalent cation, forming a bidentate complex in the Δ pseudoaxial configuration (Carlier *et al.*, 1991). This binding is possibly transduced into a tertiary structure change, presently unknown, which hampers the sideways bending of the tubulin $\alpha\beta$ dimer by 22·5° and 30° (i.e. the required angles to form the GDP-tubulin outer and inner rings), and/or facilitates the correct lateral interaction between protofilaments. Analogy with other GTP binding proteins is immediate, even though tubulin is not closely related to the GTPase superfamily (Bourne *et al.*, 1991). X-ray crystallography has shown that in the small guanosine nucleotide binding protein, ras-p21, the molecular switching between the inactive and active forms involves significant modifications in the structure of two loops which participate in the binding of the cation-γ-phosphate and form a continuous patch on the surface of the molecule (Wittinghofer & Pai, 1991). Very recently, it has been demonstrated that similar changes in the effector region of the structurally homologous nucleotide binding domain 1 of elongation factor Tu lead to major domain rearrangements, in which domains 2 and 3 of this protein come into tight contact with domain 1 in the GTP conformation, closing a cleft of the GDP liganded form (Berchtold *et al.*, 1993; Kjeldgaard *et al.*, 1993). It has been proposed that the equilibrium between the inactive and active states of tubulin (Howard & Timasheff, 1986) is actually displaced from the ring forming state to the microtubule forming state by the binding of one magnesium ion to GTP-tubulin in its active conformation (Shearwin & Timahseff, 1994). It was suggested that GDP-tubulin in the "curved" conformation does not polymerize into microtubules because the distortion free energy required to maintain a "straight" conformation is larger than the free energy of subunit addition (Shearwin & Timasheff, 1992). Inactive GDP-tubulin can be driven to assemble into microtubules by the linked binding of taxol (Díaz *et al.*, 1993*a*). Time-resolved X-ray scattering analysis of this system allows observation of intermediate steps of microtubule assembly (Díaz *et al.*, 1993*b*).

We thank the staff of Daresbury Laboratory and our colleagues Liz Towns-Andrews, Greg Diakun, Eva Nogales, Jose M. de Pereda and Vincent Peyrot for their extensive help, Jose L. Carrascosa for image analysis of tubulin ring pseudolattices, Aurelio Hurtado for the drawings, and Ricardo Uña & Jose Blanco for photography. This work was supported by DGICyT grants PB920007 and GR890021, and access to the Daresbury Synchrotron Radiation Source was obtained through the European Community Large Installations Program.

References

Abramowitz, M. & Stegun, I. A. (1965). *Handbook of Mathematical Functions*, Dover Publications, Inc., New York.

Amos, L. A. & Klug, A. (1974). Arrangement of subunits in flagellar microtubules. *J. Cell Sci.* **14**, 523–549.

Andreu, J. M., García de Ancos, J., Starling, D., Hodgkinson, J. L. & Bordas, J. (1989). A synchrotron X-ray scattering characterization of purified tubulin and of its expansion induced by mild detergent binding. *Biochemistry*, **28**, 4036–4040.

Andreu, J. M., Bordas, J., Díaz, J. F., García de Ancos, J., Gil, R., Medrano, F. J., Nogales, E., Pantos, E. & Towns-Andrews, E. (1992). Low resolution structure of microtubules in solution. Synchrotron X-ray scattering and electron microscopy of taxol-induced microtubules assembled from purified tubulin in comparison with glycerol- and Map-induced microtubules. *J. Mol. Biol.* **226**, 169–184.

Beese, L., Stubbs, G. & Cohen, C. (1987). Microtubule structure at 18 Å resolution. *J. Mol. Biol.* **194**, 257–264.

Berchtold, H., Reshetnikova, L., Reiser, C. O. A., Schrimer, N. K., Sprinzl, M. & Hilgenfeld, R. (1993). Crystal structure of active elongation factor Tu

reveals major domain rearrangements. *Nature (London)*, **365**, 126–132.

Bordas, J., Mandelkow, E. M. & Mandelkow, E. (1983). Stages of tubulin assembly and disassembly studied by time-resolved synchrotron X-ray scattering. *J. Mol. Biol.* **164**, 89–135.

Bourne, H. R., Sanders, D. & McCormick, F. (1991). The GTPase superfamily: conserved structure and molecular mechanism. *Nature (London)*, **349**, 117–127.

Carlier, M. F. (1991). Nucleotide hydrolysis in cytoskeletal assembly. *Curr. Opin. Cell. Biol.* **3**, 12–17.

Carlier, M. F., Didry, C., Melki, R., Chabre, M. & Pantaloni, D. (1988). Stabilization of microtubules by inorganic phosphate and by its structural analogues, the fluoride complexes of aluminium and beryllium. *Biochemistry*, **27**, 3555–3559.

Carlier, M. F., Didry, D. & Valentin-Ranc, C. (1991). Interaction between chromium GTP and tubulin. Stereochemistry of GTP binding, GTP hydrolysis and microtubule stabilization. *J. Biol. Chem.* **266**, 12361–12368.

Cassimeris, L. U., Pryer, N. K. & Salmon, E. D. (1988). Real time observations of microtubule dynamic instability in living cells. *J. Cell Biol.* **107**, 2223–2231.

Chen, Y. & Hill, T. L. (1985). Theoretical treatment of microtubules disappearing in solution. *Proc. Nat. Acad. Sci., U.S.A.* **82**, 4127–4131.

Correia, J. J., Beth, A. & Williams, R. C. (1988). Tubulin exchanges divalent cations at both nucleotide-binding sites. *J. Biol. Chem.* **263**, 10681–10686.

Díaz, J. F. & Andreu, J. M. (1993). Assembly of purified GDP-tubulin into microtubules induced by taxol and Taxotere: reversibility, ligand stoichiometry and competition. *Biochemistry*, **32**, 2747–2755.

Díaz, J. F., Menéndez, M. & Andreu, J. M. (1993*a*). Thermodynamics of ligand-induced assembly of tubulin. *Biochemistry*, **32**, 10067–10077.

Díaz, J. F., Andreu, J. M., Bordas, J. & Towns-Andrews, E. (1993*b*). Time-resolved X-ray scattering of ligand-induced microtubule assembly shows intermediate structures. *Abstracts 11th Int. Biophysics Congr., Budapest*, A3.113.

Erickson, H. P. & O'Brien, E. T. (1992). Microtubule dynamic instability and GTP hydrolysis. *Annu. Rev. Biophys. Biomol. Struct.* **21**, 145–166.

Frigon, R. & Timasheff, S. N. (1975*a*). Magnesium-induced self-association of calf brain tubulin. I. Stoichiometry. *Biochemistry*, **14**, 4559–4566.

Frigon, R. & Timasheff, S. N. (1975*b*). Magnesium-induced self-association of calf brain tubulin. II. Thermodynamics. *Biochemistry*, **14**, 4567–4573.

Garrigos, M., Mallam, S., Vachette, P. & Bordas, J. (1992). Structure of the myosin head in solution and effect of light chain 2 removal. *Biophys. J.* **63**, 1462–1470.

Guinier, A. & Fournet, G. (1955). *Small Angle Scattering of X-rays*. Wiley, New York.

Howard, W. D. & Timasheff, S. N. (1986). GDP state of tubulin: stabilization of double rings. *Biochemistry*, **25**, 8292–8300.

Hyman, A. A., Salser, S., Dreschel, D. N., Unwin, N. & Mitchison, T. J. (1992). Role of GTP hydrolysis in microtubule dynamics: information from a slowly hydrolyzable analogue, GMPCPP. *Mol. Biol. Cell*, **3**, 1155–1167.

Kirschner, M. W., Williams, R. C., Weingarten, M. & Gerhart, J. C. (1974). Microtubules from mammalian brain: some properties of their depolymerization products and proposed mechanism of assembly and disassembly. *Proc. Nat. Acad. Sci., U.S.A.* **71**, 1159–1163.

Kirschner, M. W. & Mitchison, T. J. (1986). Beyond self assembly: from microtubules to morphogenesis. *Cell*, **45**, 329–342.

Kjelgaard, M., Nissen, P., Thirup, S. & Nyborg, J. (1993). The crystal structure of elongation factor EF-Tu from *Thermus aquaticus* in the GTP conformation. *Structure*, **1**, 35–50.

Koch, M. H. J. & Bendall, P. (1981). Proc. Digital Equipment Computer User Society DECUS, U.K., pp. 13–16.

Lee, J. C. & Timasheff, S. N. (1975). The reconstitution of microtubules from purified calf brain tubulin. *Biochemistry*, **14**, 5183–5187.

Mandelkow, E., Thomas, J. & Cohen, C. (1977). Microtubule structure at low resolution by X-ray diffraction. *Proc. Nat. Acad. Sci., U.S.A.* **74**, 3370–3374.

Mandelkow, E., Mandelkow, E. M. & Bordas, J. (1983). Structure of tubulin rings studied by X-ray scattering using synchrotron radiation. *J. Mol. Biol.* **167**, 179–196.

Mandelkow, E. M., Mandelkow, E. & Milligan, R. A. (1991). Microtubule dynamics and microtubule caps: a time-resolved cryo-electron microscopy study. *J. Cell Biol.* **114**, 977–991.

Martin, S. R., Schlistra, M. J. & Bayley, P. M. (1993). Dynamic instability of microtubules: Monte Carlo simulation and application to different types of microtubule lattice. *Biophys. J.* **65**, 578–596.

Melki, R., Carlier, M. F., Pantaloni, D. & Timasheff, S. N. (1990). Cold depolymerization of microtubules to double rings: geometric stabilization of assemblies. *Biochemistry*, **28**, 9143–9152.

Mitchison, T. J. (1993). Localization of an exchangeable GTP binding site at the plus end of microtubules. *Science*, **261**, 1044–1047.

Pantos, E. & Bordas, J. (1994). Supercomputer simulation of small angle X-ray scattering, electron micrographs and X-ray diffraction patterns of macromolecular structures. *J. Pure Appl. Chem.* **66**, 77–82.

Pantos, E., Mant, G. R., Starling, D., Jones, G. R. & Bordas, J. (1988). Three dimensional structure simulation: application to electron microscopy and X-ray diffraction data. Proc. 2nd Int. Conf. on Biophysics and Synchrotron Radiation, Chester, pp. 205–208.

Ray, S., Meyhöfer, E., Milligan, R. A. & Howard, J. (1993). Kinesin follows the microtubule's protofilament axis. *J. Cell Biol.* **121**, 1083–1093.

Scheele, R. B. & Borisy, G. G. (1978). Electron microscopy of metal-shadowed and negatively stained microtubule protein. Structure of the 30 S oligomer. *J. Biol. Chem.* **253**, 2846–2851.

Shearwin, K. E. & Timasheff, S. N. (1992). Linkage between ligand binding and control of tubulin conformation. *Biochemistry*, **31**, 8080–8089.

Shearwin, K. E. & Timasheff, S. N. (1994). Linkages between the dissociation of $\alpha\beta$ tubulin into subunits and ligand binding; the ground state of tubulin is the GDP conformation. *Biochemistry*, **33**, 885–893.

Simon, J. R. & Salmon, E. D. (1990). The structure of microtubule ends during the elongation and shortening phases of dynamic instability examined by negative-stain electron microscopy. *J. Cell Sci.* **96**, 571–582.

Timasheff, S. N. (1990). The role of double rings in the tubulin-microtubule cycle: linkage with nucleotide binding. *AIP Conf. Proc.* **226**, 170–180.

Towns-Andrews, E., Berry, A., Bordas, J., Mant, G. R., Murray, P. K., Roberts, K., Sumner, I., Worgan, J. S., Lewis, R. & Gabriel, A. (1989). A time-resolved X-ray diffraction station: X-ray optics, detectors and data acquisition. *Rev. Sci. Instrum.* **60**, 2346–2349.

Vainshtein, B. K. (1966). *Diffraction of X-rays by Chain Molecules*. Elsevier, Amsterdam.

Verde, F., Dogterom, M., Stelzer, E., Karsenti, E. & Leibler, S. (1992). Control of microtubule dynamics and length by cyclin A and cyclin B dependent kinase in *Xenopus* egg. *J. Cell Biol.* **118**, 1098–1108.

Voter, W. A. & Erickson, H. P. (1979). Tubulin rings: curved filaments with limited flexibility and two modes of association. *J. Supramol. Struct.* **10**, 419–431.

Wade, R. H., Pirollet, F., Margolis, R. L., Garel, J. R. & Job, D. (1989). Monotonic *versus* oscillating microtubule assemble: a cryo-electron microscopy study. *Biol. Cell*, **65**, 37–44.

Wade, R. H., Chrétien, D. & Job, D. (1990). Characterization of microtubule protofilament numbers. How does the surface lattice accommodate? *J. Mol. Biol.* **212**, 775–786.

Wakabayashi, K., Tokunaga, M., Kohno, I., Sugimoto, Y., Hamanaka, T., Takezawa, Y., Wakabayashi, T. & Anemiya, Y. (1992). Small-angle synchrotron X-ray scattering reveals distinct shape changes of the myosin head during hydrolysis of ATP. *Science*, **258**, 443–447.

Wittinghofer, A. & Pai, E. F. (1991). The structure of Ras protein: a model for a universal molecular switch. *Trends Biochem. Sci.* **16**, 382–387.

Edited by V. Luzzati

(Received 28 November 1993; accepted 3 February 1994)

APPENDIX

Hydrodynamic Analysis of Tubulin Dimer and Double Rings

Jose García de la Torre[1] and Jose M. Andreu[2]

[1]*Departamento de Química Física, Fac. Química Universidad de Murcia, 30071 Murcia, Spain*

[2]*Centro de Investigaciones Biológicas, C.S.I.C Velazquez 144, 28006 Madrid, Spain*

This Appendix describes rigorous calculations of the sedimentation coefficients of the bead models of tubulin monomer, dimer and double rings employed in the X-ray scattering analysis of GDP-tubulin rings (Díaz *et al.*, 1994). In their elegant study of magnesium-induced tubulin self-association, Frigon & Timasheff (1975) carried out an early hydrodynamic analysis of the tubulin dimer, analyzed in terms of a hydrated anisometric ellipsoid, and of the 42 S double-ring end product. The tubulin double ring structure was simplified to a single plane polygon, of dimensions estimated by electron microscopy, having a frictional unit at each vertex with the experimental frictional coefficient and molecular weight of a tubulin dimer. The hydrodynamic calculation was based on the Kirkwood (1954) formula, well known to be a simple approximation. Zwanzig (1966) showed that for rings with many units this formula underestimates the frictional coefficient (or overestimates the sedimentation coefficient) up to 8%. The conclusion that tubulin rings are made of 26 ± 2 tubulin dimers (Frigon & Timasheff, 1975) is compatible with the X-ray scattering analysis, however, accurate discrimination between models with different number of monomers per ring was not possible. In the present analysis the hydrodynamics of the tubulin dimer is characterized based on the X-ray scattering model and its experimental sedimentation coefficient, and the approximate frictional coefficient of the tubulin monomer is extracted. Then the sedimentation coefficients of the pertinent X-ray double ring models are calculated with rigorous hydrodynamic theory, employing the molecular weight and frictional coefficient of the monomer and the double ring dimensions determined by X-ray scattering. The results strongly support the X-ray scattering analysis and allow selection of the number of tubulin subunits in each ring.

(a) *Hydrodynamic computer modelling and experimental parameters*

The calculation of sedimentation coefficients and other solution properties has been carried out employing the most advanced versions of the hydrodynamic theory and computer programs for multisubunit structures (García de la Torre & Bloomfield,

Table A1

Hydrodynamic properties of tubulin dimer, monomer and double ring bead models

	Dimer	Monomer		Double ring			
				$s^{\circ}_{20,w}$ (S)			
Bead radius (nm)	$s^{\circ}_{20,w}$† (S)	$s^{\circ}_{20,w}$ (S)	$f_1 \times 10^8$‡ (cgs units)	Number of monomers per ring (n_1+n_2) 30+22	32+24	34+26	36+28
1·2	6·49	4·16	5·80	39·9	42·9	45·9	48·9
1·4	6·17	3·91	6·16	39·4	42·4	45·3	48·3
1·6	5·89	3·70	6·52	38·9	41·9	44·8	47·8
1·7	5·75	3·60	6·69	38·7	41·6	44·6	47·5
1·8	5·63	3·51	6·87	38·5	41·4	44·3	47·3
1·9	5·51	3·42	7·05	38·3	41·2	44·1	47·0

† Sedimentation coefficient.
‡ Frictional coefficient.

1980; García de la Torre, 1989, 1992). For the detailed structure of the non-globular tubulin units, the Cartesian coordinates of the small spherical beads, as obtained from the X-ray scattering simulation software, were used directly in the hydrodynamics programs.

The tubulin dimer has a sedimentation coefficient $s^{\circ}_{20,w} = 5{\cdot}8$ S, a partial specific volume of 0·736 ml g^{-1}, and molecular mass $M_r = 2 \times 50{,}000$ (Lee *et al.*, 1973; Frigon & Timasheff, 1975; Howard & Timasheff, 1986; Shearwin & Timasheff, 1992; Rivas & Andreu, unpublished results), experimentally determined employing the same purified protein under conditions similar to the X-ray scattering study. This gives a frictional coefficient $f = 8{\cdot}3 \times 10^{-8}$ cgs units. Similarly, the sedimentation coefficient of tubulin rings is $s^{\circ}_{20,w} = 42 \pm 2$ S (Frigon & Timasheff, 1975), a value shown to be independent of having GDP or GTP at the exchangeable nucleotide site of the protein and refined to 42 ± 1 S with colchicine-liganded tubulin (Howard & Timasheff, 1986; Shearwin & Timasheff, 1992).

(b) *Tubulin dimer and monomer*

The hydrodynamic dimer model was obtained from the X-ray scattering model of tubulin rings (Díaz *et al.*, 1994), by taking a set of 42 spheres corresponding to two adjacent monomeric units, each made of 21 spheres of radius $r = 1{\cdot}2$ nm, with the above molecular mass. The calculated sedimentation coefficient for the dimer is $s^{\circ}_{20,w} = 6{\cdot}5$ S, which is 12% larger than the experimental value of 5·8 S. A slight overestimation such as this can be well explained in terms of hydration. Estimating hydration as about 0·36 g water per g tubulin (Frigon & Timasheff, 1975) amounts roughly to an increase in the main dimensions of the hydrated particle with respect to the anhydrous one of about 12%. In models of arbitrary shape made up of beads, a possible way to account for hydration effects is through the radius of the beads. This parameter can be increased beyond the values that the beads in the model would have if they were just touching their neighbours, while keeping the molecular mass constant. Actually, the theory and computer programs employed embody the hydrodynamic interaction tensor that accounts for this possibility (Rotne & Prager, 1970; Yamakawa, 1970). This way, in a series of calculations, the bead radius was increased beyond the 1·2 nm value used in scattering modelling. For an appreciably larger value such as, for instance, $r = 1{\cdot}6$ nm, the increase in the main dimensions of the particle would be $2 \times (1{\cdot}6 - 1{\cdot}2)$ nm = 0·8 nm. From the X-ray scattering model structure (the size of the monomer is roughly 4 nm × 7 nm × 8 nm), the relative size increase averaged over the three inertial axes would be 13%, which is compatible with the above estimate from hydration.

The results of the series of calculations for the dimer are shown in Table A1. We note that the experimental sedimentation coefficient value can be accurately reproduced by the calculations for $1{\cdot}6 < r < 1{\cdot}7$ nm, which is a quite reasonable choice as discussed above. Allowing for an admissible error in the sedimentation coefficient, for example, taking as experimental value 5·6 S (Andreu & Muñoz, 1986), would yield a larger but not unreasonable value, $1{\cdot}8 < r < 1{\cdot}9$ nm, for the bead radius of the model. Therefore, it is possible to simulate the experimental sedimentation coefficient of the dimer using the very same X-ray scattering model in the hydrodynamic analysis.

The hydrodynamic properties of the monomer can be estimated by a similar calculation, for a model of 21 beads for the subunit taken from the X-ray model of the whole double ring. The values obtained for the friction and sedimentation coefficient ($M_r = 55{,}000$) are listed in Table A1. The experimental sedimentation coefficient of the tubulin monomers is not presently available. Though it has been assumed for the purpose of the hydrodynamic analysis that the tubulin dimer has similar shape in its unassembled and assembled states, it may also be considered that the structure of tubulin should differ in the different aggregation states. Employing a tubulin dimer taken from

microtubule models, instead of ring models, gave a very small change in the calculated sedimentation coefficient. Therefore, these differences have been ignored in the first approximation. A more exact analysis would require more detailed X-ray modelling of the tubulin monomer in its different association states.

(c) *Tubulin double rings*

The tubulin double rings have been modelled for hydrodynamic purposes by regular concentric polygons of n_1 and n_2 vertices, which are occupied by monomeric units having molecular mass 55,000 Da and friction coefficient f_1. For the latter parameter any of the plausible values estimated (listed in Table A1) can be taken. The radii of the outer and inner rings are constrained to the respective values 21·8 nm and 16·2 nm, determined by X-ray scattering (Díaz *et al.*, 1994), and calculation of the Cartesian coordinates of the vertices of the polygons is trivial. This has been done with several choices for the numbers of monomers in each ring, n_1+n_2, namely 30+22, 32+24, 34+26 and 36+28 (corresponding to 26, 28, 30 and 32 tubulin dimers). The calculated sedimentation coefficients of the double rings are shown in Table A1. The values obtained for the case with 32+24 subunits are in excellent agreement with the experimental data, $s^\circ_{20,w} = 42 \pm 1$ S. The calculated coefficient of rings is rather insensitive to the choice of f_1, in contrast to the case of the dimer. Particularly, for the same values of $f_1 = (6{\cdot}52\text{–}6{\cdot}69) \times 10^{-8}$ cgs units that reproduce the experimental $s^\circ_{20,w}$ of the dimer, we calculate for the double ring $s^\circ_{20,w} = 41{\cdot}9$ to 41·6 S, which is coincident with the experimental result. For the other choices of n_1+n_2, it can be observed that, regardless of the tabulated value of f_1, the calculated values differ from the experimental result beyond the error of the latter.

In conclusion, X-ray scattering analysis of GDP-tubulin double rings plus rigorous hydrodynamic treatment gives a fully accurate description of the experimental sedimentation values, and strongly favours the 32+24 monomer double ring model.

This work was supported by DGICyT grants PB900303 and PB920007.

References

Andreu, J. M. & Muñoz, J. A. (1986). Interaction of tubulin with octyl glucoside and deoxycholate. 1. Binding and hydrodynamic studies. *Biochemistry*, **25**, 5220–5230.

Díaz, J. F., Pantos, E., Bordas, J. & Andreu, J. M. (1994). Solution structure of GDP-tubulin double rings to 3 nm resolution and comparison with microtubles. *J. Mol. Biol.* **238**, 214–223.

Frigon, R. P. & Timasheff, S. N. (1975). Magnesium-induced self-association of calf brain tubulin. I. Stoichiometry. *Biochemistry*, **14**, 4559–4566.

García de la Torre, J. (1989). Hydrodynamic properties of macromolecular assemblies. In *Dynamic Properties of Biomolecular Assemblies* (Harding, S. E. & Rowe, A. J., eds), pp. 3–31, The Royal Society of Chemistry, Cambridge.

García de la Torre, J. (1992). Sedimentation coefficients of complex biological particles. In *Analytical Ultracentrifugation in Biochemistry and Polymer Science* (Harding, S. E., Rowe, A. J. & Horton, J. C., eds), pp. 333–345, The Royal Society of Chemistry, Cambridge.

García de la Torre, J. & Bloomfield, V. A. (1980). Hydrodynamic properties of complex, rigid, biological macromolecules. Theory and applications. *Quart. Rev. Biophys.* **14**, 81–139.

Howard, W. D. & Timasheff, S. N. (1986). GDP state of tubulin: stabilization of double rings. *Biochemistry*, **25**, 8292–8300.

Kirkwood, J. G. (1954). The general theory of irreversible processes in solutions of macromolecules. *J. Polymer Sci.* **12**, 1–14.

Lee, J. C., Frigon, R. P. & Timasheff, S. N. (1973). The chemical characterization of calf brain microtubule protein subunits. *J. Biol. Chem.* **248**, 7253–7262.

Rotne, J. & Prager, S. (1970). Variational treatment of hydrodynamic interaction in polymers. *J. Chem. Phys.* **50**, 4831–4837.

Shearwin, K. E. & Timasheff, S. N. (1992). Linkage between ligand binding and control of tubulin conformation. *Biochemistry*, **31**, 8080–8089.

Yamakawa, H. (1970). Transport properties of polymer chains in dilute solution: hydrodynamic interaction. *J. Chem. Phys.* **53**, 436–443.

Zwanzig, R. (1966). Translational diffusion in polymer solutions. *J. Chem. Phys.* **45**, 1858–1860.